Pion Form Factor with Overlap Fermion

Gen Wang[*]

Dept. of Physics and Astronomy, University of Kentucky, Lexington, KY 40506, USA
E-mail: genwang27@uky.edu

Jian Liang

Dept. of Physics and Astronomy, University of Kentucky, Lexington, KY 40506, USA
E-mail: jian.liang@uky.edu

Terrence Draper

Dept. of Physics and Astronomy, University of Kentucky, Lexington, KY 40506, USA
E-mail: draper@pa.uky.edu

Keh-Fei Liu

Dept. of Physics and Astronomy, University of Kentucky, Lexington, KY 40506, USA
E-mail: liu@pa.uky.edu

Yi-Bo Yang

Institute of Theoretical Physics, Chinese Academy of Sciences, Beijing 100190, China
E-mail: ybyang@itp.ac.cn

(χQCD Collaboration)

We present a calculation of the pion form factor using overlap fermions on 2+1-flavor domain-wall configurations on a $24^3 \times 64$ lattice with $a = 0.11\,\mathrm{fm}$ and on a $32^3 \times 64$ lattice with $a = 0.143\,\mathrm{fm}$ generated by the RBC/UKQCD collaboration. Using the multi-mass algorithm, a simulation has been done with various valence quark masses with a range of space-like Q^2 from 0.0 to 0.6 GeV^2.

---

[*]Speaker.

1. Introduction

The charged pion electromagnetic form factor can be probed by a vector current of the photon. The experimental error of the pion electromagnetic form factor is around 1% in the small q^2 region with mean squared radius $\langle r^2 \rangle = 0.452(11)$ fm^2 as given by the Particle Data Group (PDG) [1]. Such a form factor can be calculated using Lattice QCD, but a precise measurement using Lattice QCD near the physical pion mass will be needed to control dominant systematic errors coming from its strong quark mass dependence. Decades of improving computational power along with the development of Lattice QCD theory and algorithms makes it possible to carry out a measurement from higher pion mass to the physical region [2, 3, 4, 5, 6, 7, 8, 9] with various actions. It has been observed that in these calculations the values of $\langle r^2 \rangle$ at higher pion masses are significantly lower than the experimental value before chiral extrapolation [10]. On the other hand, one calculation using Highly Improved Staggered Quark formalism [9] directly at the physical pion mass agrees with experiment.

In order to study the above strong quark mass dependence of the pion form factor, the overlap fermion with multi-mass algorithm will be a good option compared to other formulations. By using existing grid source propagators with several quark masses generated by our χQCD collaboration using overlap fermions, a straightforward calculation of the vector current three-point functions and corresponding two-point functions has been carried out to obtain $\langle r^2 \rangle$ with less than 4% error at several valence pion masses ranging from 147 MeV to 389 MeV on two lattices.

2. Lattice Setup and Fitting Results

In this work, we use overlap fermions on 2+1-flavor domain-wall configurations on a $24^3 \times 64$ lattice (24I) with Iwasaki gauge action and on a $32^3 \times 64$ lattice (32ID) with Iwasaki plus the Dislocation Suppressing Determinant Ratio (DSDR) gauge action [11] listed in Table 1. For pion correlation functions, grid sources without low mode substitution (LMS) have been used in this production as suggested in reference [12]. With a careful treatment of the backward pion propagation, we are able to use two time sources with separation of half of total number of time slices ($T/2$) to double the statistics. On 24I, a Gaussian-smeared source [13] has been applied with root mean square (RMS) radius 1.18 fm along with the same smeared sink. On 32ID, a box-smeared source [14] has been applied with box half size 1.0 fm along with the same smeared sink. Such a two-point function will be fitted using Eq. (2.1).

$$
\begin{aligned}
C_{2pt}(t, \vec{p}) &= \sum_{\vec{x}} e^{-i\vec{p}\cdot\vec{x}} \langle \mathrm{T}[\chi_{\pi^+}(\vec{x}, t) \chi_{\pi^+}^\dagger(\vec{0}, [0, T/2])] \rangle \\
&\approx \frac{m|Z_{\vec{p}}|^2}{E} (e^{-Et} + e^{-E(T/2-t)})(1 + e^{-E(T/2)}) \\
&\quad + \frac{m|Z_{\vec{p}}^1|^2}{E^1} (e^{-E^1 t} + e^{-E^1(T/2-t)})(1 + e^{-E^1(T/2)})
\end{aligned}
\tag{2.1}
$$

$\chi_{\pi^+}(\vec{x}, t) = \bar{u}(\vec{x}, t)\gamma_5 d(\vec{x}, t)$ is the interpolating field of the pion, E is the pion energy at momentum $\vec{p}$ and $Z_{\vec{p}}$ is the spectral weight for smeared source and sink at momentum $\vec{p}$ and E^1 and $Z_{\vec{p}}^1$ are the corresponding energy and spectral weight of the first excited state.

Lattice	Size	a (fm)	L (fm)	Pion (MeV)	$m_\pi L$
24I	$24^3 \times 64$	0.11	2.64	337	4.5
32ID	$32^3 \times 64$	0.143	4.58	171	3.97

Table 1: Lattice parameters of 24I and 32ID

Precise simulation of the three-point functions with connected-inserstion of vector current V_4 for the matrix element $\langle \pi(p_f) | V_4 | \pi(p_i) \rangle$ has been done with the stochastic sandwich method described in reference [15]. Along with sink momentum $\vec{p}_f = 0$ and mixed momentum source [15] with momentum $\vec{p}_i$ equal to momentum transfer $\vec{q} = \vec{p}_f - \vec{p}_i$, we can code with the same trick as the sink-sequential method [16, 17] to determine all the momentum transfers with only one three-point function contraction to significantly lower the contraction cost. The corresponding three-point function can be fitted with Eq. (2.2)

$$
\begin{aligned}
C_{3pt}(\tau, t_f, \vec{p}_i, \vec{p}_f) &= \sum_{\vec{x}_f, \vec{z}} e^{-i\vec{p}_f \cdot (\vec{x}_f - \vec{z})} e^{-i\vec{p}_i \cdot \vec{z}} \langle T[\chi_{\pi^+}(\vec{x}_f, t_f) V_4(\vec{z}, \tau) \chi_{\pi^+}^\dagger(\vec{0}, [0, T/2])] \rangle \\
&\approx \frac{Z_{\vec{p}_i} Z_{\vec{p}_f} (2m)^2}{(La)^3 4 E_i E_f} \langle \pi(p_f) | V_4 | \pi(p_i) \rangle \\
&\quad \times e^{-E_i \tau - E_f(t_f - \tau)} (1 + e^{-E_i T/2}) \\
&\quad + C_1 e^{-E_i^1 \tau - E_f^1(t_f - \tau)} + C_2 e^{-E_i^1 \tau - E_f^1(t_f - \tau)}
\end{aligned}
$$

(2.2)

in which common parameters have the same meaning as in the two-point function, E_i and E_f are the pion energy at momentum $\vec{p}_i$ and $\vec{p}_f$ and E_i^1 and E_f^1 are the corresponding energies of the first excited state. C_1 and C_2 are the unknown transition amplitudes with corresponding overlap factors from ground state to the first excited state as $\langle \pi^1(p_f) | V_4 | \pi(p_i) \rangle$ and $\langle \pi(p_f) | V_4 | \pi^1(p_i) \rangle$, respectively. We ignore the matrix element $\langle \pi^1(p_f) | V_4 | \pi^1(p_i) \rangle$ which is small in most cases. By using the same smeared source and smeared sink as in the two-point function, joint fitting of C_{3pt} and C_{2pt} can give the matrix elements $\langle \pi(p_f) | V_4 | \pi(p_i) \rangle$ at several momentum transfers. In order to control the systematic errors coming from the excited-state contamination, we have done calculations with source-sink separation $t_f - t_i = 8a, 10a$ and $12a$ on 24I (equal to 0.88 fm, 1.10 fm and 1.32 fm, respectively) and $t_f - t_i = 9a, 10a$ and $11a$ on 32ID (equal to 1.287 fm, 1.430 fm and 1.573 fm, respectively). As an example, Fig. 1 shows the fitting plot on 32ID for pion mass 174 MeV at zero momentum transfer and pion form factor $f_{\pi\pi}(Q^2)$ from Eq. (2.3) at the smallest momentum transfer with $Q^2 \equiv q^2 - (E_f - E_i)^2 = 0.05$ GeV^2 with reasonable χ^2 of $0.6 - 1.2$. The result shows only a 0.5% difference between separations which means that the current source-sink separations are large enough so that there is a good control of the systematic errors from the excited-state contamination.

$$
f_{\pi\pi}(Q^2) = \frac{1}{E_i + E_f} \frac{\langle \pi(p_f) | V_4 | \pi(p_i) \rangle}{\langle \pi(p_f) | V_4 | \pi(p_f) \rangle}
$$

(2.3)

As we are using overlap fermions which have exact chiral symmetry on lattice, we should have vector renormalization constant equal to axial normalization constant, $Z_V = Z_A$. A detailed study of renormalization constants of overlap quark bilinear operators [18] shows that $Z_V / Z_A = 1$ is well
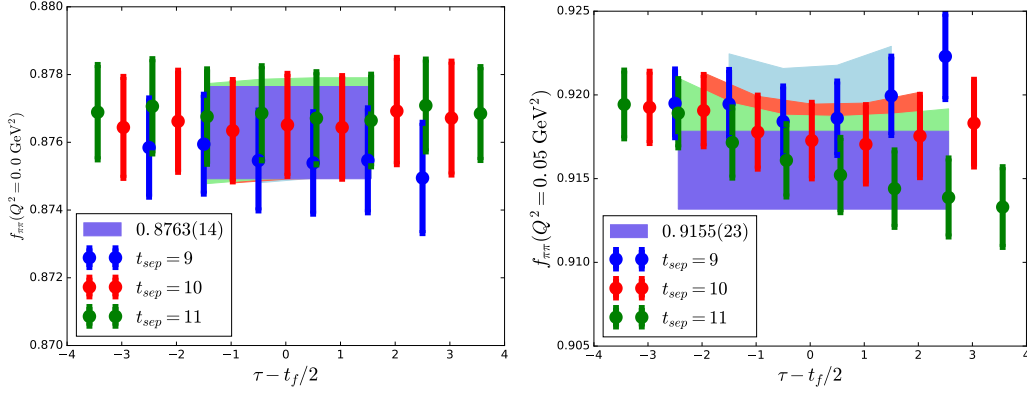
Figure 1: (Left panel) The joint fitting of correlation functions on 32ID at zero momentum transfer. (Right panel) The case of $p_x = 0, p_y = 0, p_z = 2\pi/L$ with the summation of 8 symmetric momenta which give momentum transfer $Q^2 = 0.05 \text{ GeV}^2$ on the 32ID at pion mass 174 MeV.

satisfied. In reference [19], Z_A has been calculated using the same method in reference [18] on the 32ID lattice. In this pion form factor calculation on 32ID, Z_V can be obtained using Eq. (2.4).

$$Z_V = \frac{1}{\langle \pi(0)|V_4|\pi(0)\rangle} \tag{2.4}$$

By comparing the Z_A from ratios of the two-point functions along with the Z_V at seven pion masses from the joint fit of the three-point function and the two-point function in Fig. 2 on 32ID, it is obvious that within 0.3% error, Z_V and Z_A agree with each other. With these two different independent analyses, we confirm that current calculation and the joint fitting analyses have good control of various systematic errors.
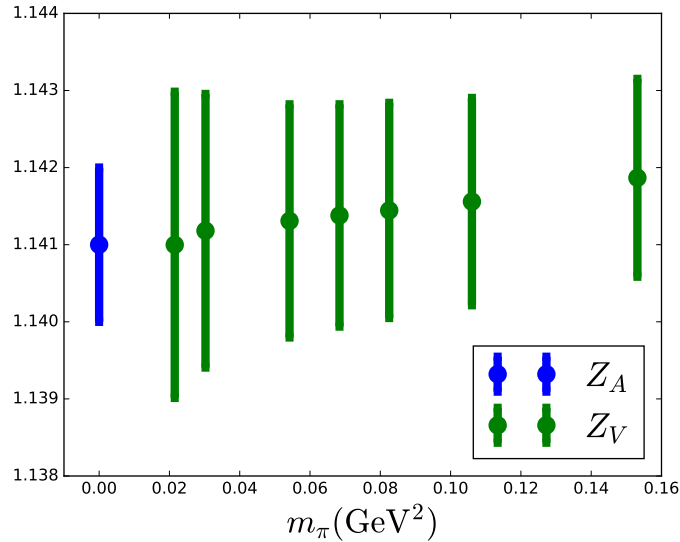

Figure 2: Z_A and Z_V on 32ID

With the *z*-expansion [20] method we have done a model-independent fitting of the pion form

Lattice	Pion (MeV)						
24I			253.26(47)	281.56(44)	320.72(43)	347.38(42)	388.92(42)
32ID	146.66(19)	173.95(18)	232.75(17)	261.50(17)	287.28(17)	325.68(17)	391.34(17)

Table 2: Fitted pion masses on 24I and 32ID

factor $f_{\pi\pi}(Q^2)$ using Eq. (2.5) with $k_{max} = 2$.

$$f_{\pi\pi}(Q^2) = 1 + \sum_{k=1}^{k_{max}} a_k z^k$$
$$z(t, t_{cut}, t_0) = \frac{\sqrt{t_{cut} - t_0} - \sqrt{t_{cut} - t_0}}{\sqrt{t_{cut} - t_0} + \sqrt{t_{cut} - t_0}} \qquad (2.5)$$
$$t = -Q^2, t_{cut} = 4m_\pi^2$$

The pion form factor results are shown in Fig. 3 with pion mass 347 MeV on 24I and 174 MeV on 32ID chosen to be close to their domain-wall sea pion mass. We have used Z_V to normalize the form factors at non-zero momentum transfers. With increasing momentum transfers, signals of the matrix elements decrease dramatically so that we can have six or seven momentum transfers which constrain the current fitting parameters. This limits our ability to access higher momenta on coarser and larger lattices such as 32ID compared to 24I.
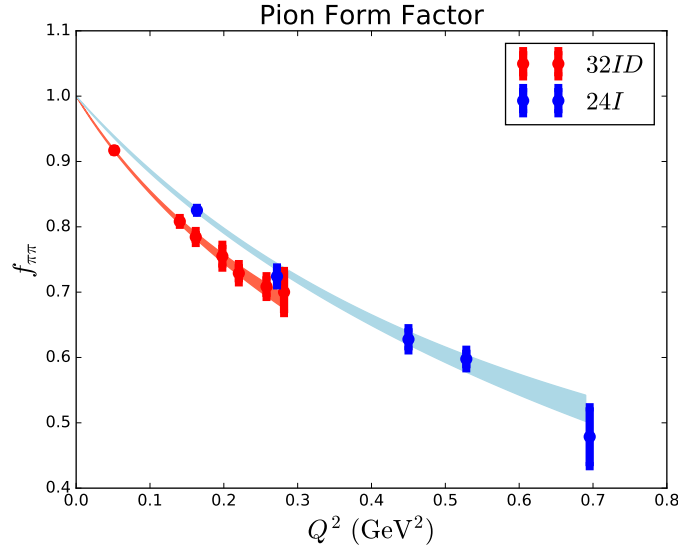

Figure 3: *z*-expansion fitting of the pion form factor on 24I with pion mass 347 MeV and on 32ID with pion mass 174 MeV.

A similar fitting procedure has been done on all valence pion masses listed in Table 2. After the *z*-expansion fitting, we can get $\langle r^2 \rangle$ by taking the derivative of the fitted function Eq. (2.6).

$$\langle r^2 \rangle \equiv 6 \frac{f_{\pi\pi}(Q^2)}{dQ^2} |_{Q^2=0} \qquad (2.6)$$

The final $\langle r^2 \rangle$ results on 24I and 32ID are shown in Fig. 4 with several pion masses including
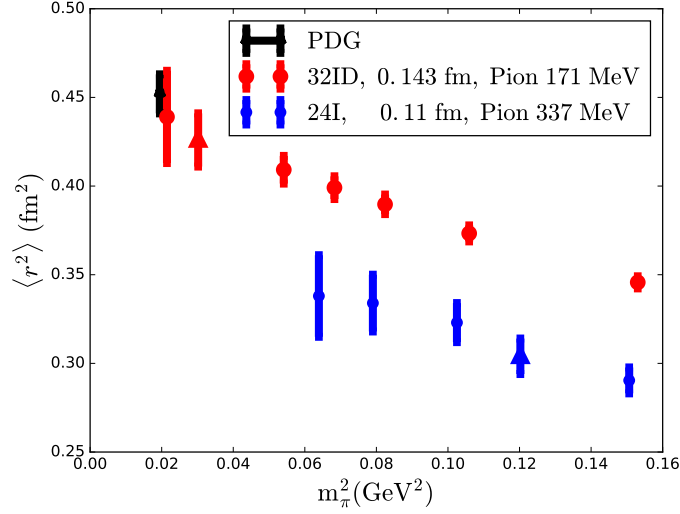
Figure 4: $\langle r^2 \rangle$ as function of m_π^2 on 24I and 32ID compared to the PDG value

146.66(19) MeV which is very close to physical pion mass 139.57 MeV. Such lowest pion mass result from 32ID is consistent with the experiment (PDG) value within current statistics. The most notable difference is that the 24I result is around 20% lower than the 32ID result at similar pion mass. Such a difference may come from their difference of sea pion mass, lattice spacing or lattice volume which is out of control in the current calculation. Due to such a large discrepancy, we will need one or two more comparable lattices to find out which parameter has the largest effect.

3. Summary and Conclusion

We presented calculations of the pion form factor using overlap fermions with a range of pion masses. By differentiating the fitted $f_{\pi\pi}(Q^2)$ shown in Fig. 3, we get the corresponding pion charge radius $\langle r^2 \rangle$ to be 0.304(10) fm^2 on 24I at pion mass 347.38(42) MeV and 0.426(15) fm^2 on 32ID at pion mass 146.66(19) MeV. With multi-mass algorithm using overlap fermions, we obtained the dependence between pion charge radius and valence pion masses shown in Fig. 4. Further calculations on additional lattices with different sea quark masses, lattice spacings and lattice volumes will be needed to do a global fitting to extrapolate to the physical limit.

References

[1] Particle Data Group, M. Tanabashi *et al.*, *Review of Particle Physics*, Phys. Rev. D **98**, 030001 (2018).

[2] D. Brömmel *et al.*, *The Pion Form Factor from Lattice QCD with Two Dynamical Flavours*, The European Physical Journal C **51**, 335 (2007), hep-lat/0608021.

[3] P. A. Boyle *et al.*, *The Pion's Electromagnetic Form Factor at Small Momentum Transfer in Full Lattice QCD*, Journal of High Energy Physics **2008**, 112 (2008), 0804.3971.

[4] O. H. Nguyen, K.-I. Ishikawa, A. Ukawa, and N. Ukita, *Electromagnetic Form Factor of Pion from N_f=2+1 Dynamical Flavor QCD*, Journal of High Energy Physics **2011** (2011), 1102.3652.

[5] J. Collaboration *et al.*, *Pion Form Factors in the Epsilon Regime*, arXiv:1211.0743 [hep-lat] (2012), 1211.0743.

[6] G. S. Bali *et al.*, *Nucleon Mass and Sigma Term from Lattice QCD with Two Light Fermion Flavors*, Nuclear Physics B **866**, 1 (2013), 1206.7034.

[7] B. B. Brandt, A. Juttner, and H. Wittig, *The Pion Vector Form Factor from Lattice QCD and NNLO Chiral Perturbation Theory*, Journal of High Energy Physics **2013** (2013), 1306.2916.

[8] J. Collaboration *et al.*, *Light Meson Electromagnetic Form Factors from Three-Flavor Lattice QCD with Exact Chiral Symmetry*, Physical Review D **93** (2016), 1510.06470.

[9] J. Koponen, F. Bursa, C. T. H. Davies, R. J. Dowdall, and G. P. Lepage, *The Size of the Pion from Full Lattice QCD with Physical u, d, s and c Quarks*, Physical Review D **93** (2016), 1511.07382.

[10] B. B. Brandt, *The Electromagnetic Form Factor of the Pion: Results from the Lattice*, International Journal of Modern Physics E **22**, 1330030 (2013), 1310.6389.

[11] P. A. Boyle *et al.*, *The Low Energy Constants of $SU(2)$ Partially Quenched Chiral Perturbation Theory from $N_{f}=2+1$ Domain Wall QCD*, Physical Review D **93** (2016), 1511.01950.

[12] A. Li *et al.*, *Overlap Valence on 2+ 1 Flavor Domain Wall Fermion Configurations with Deflation and Low-Mode Substitution*, Physical Review D **82**, 114501 (2010).

[13] T. A. DeGrand and R. D. Loft, *Wave-Function Tests for Lattice QCD Spectroscopy*, Computer Physics Communications **65**, 84 (1991).

[14] C. R. Allton, C. T. Sachrajda, V. Lubicz, L. Maiani, and G. Martinelli, *A Lattice Computation of the Decay Constant of the B-Meson*, Nuclear Physics B **349**, 598 (1991).

[15] χQCD Collaboration *et al.*, *Stochastic Method with Low Mode Substitution for Nucleon Isovector Matrix Elements*, Physical Review D **93**, 034503 (2016).

[16] C. Bernard, T. Draper, G. Hockney, A. M. Rushton, and A. Soni, *Lattice Calculation of Weak Matrix Elements*, Physical Review Letters **55**, 2770 (1985).

[17] G. Martinelli and C. T. Sachrajda, *A Lattice Study of Nucleon Structure*, Nuclear Physics B **316**, 355 (1989).

[18] χQCD Collaboration *et al.*, *RI/MOM and RI/SMOM Renormalization of Overlap Quark Bilinears on Domain Wall Fermion Configurations*, Physical Review D **97**, 094501 (2018).

[19] J. Liang, Y.-B. Yang, T. Draper, M. Gong, and K.-F. Liu, *Quark Spins and Anomalous Ward Identity*, arXiv:1806.08366 [hep-lat, physics:hep-ph] (2018), 1806.08366.

[20] G. Lee, J. R. Arrington, and R. J. Hill, *Extraction of the Proton Radius from Electron-Proton Scattering Data*, Physical Review D **92** (2015), 1505.01489.